

Vibrationally coupled electron transport in single-molecule junctions: The importance of electron-hole pair creation processes

R. Härtle^{*1}, U. Peskin², M. Thoss³

¹ Department of Physics, Columbia University, 538 West 120th Street, New York, NY 10027, USA.

² Schulich Faculty of Chemistry and the Lise Meitner Center for Computational Quantum Chemistry, Technion-Israel Institute of Technology, Haifa 32000, Israel.

³ Institut für Theoretische Physik und Interdisziplinäres Zentrum für Molekulare Materialien, Friedrich-Alexander-Universität Erlangen-Nürnberg, Staudtstr. 7/B2, D-91058 Erlangen, Germany.

Received XXXX, revised XXXX, accepted XXXX

Published online XXXX

Key words: molecular electronics, electronic-vibrational coupling, vibrationally coupled electron transport, electron-hole pair creation, nonequilibrium Greensfunction theory

* Corresponding author: e-mail rh2613@columbia.edu, Phone: +xx-xx-xxxxxxx, Fax: +xx-xx-xxx

Vibrationally coupled electron transport through single-molecule junctions is considered. Reviewing our recent theoretical work, we show that electron-hole pair creation processes represent the key to understand the vibrational excitation characteristic of a single-molecule contact. Moreover, these processes can lead to a number of interesting transport phenomena such as, for example, negative differential resistance, rectification, mode-se-

lective vibrational excitation and a pronounced temperature dependence of the electrical current. Thus, electron-hole pair creation processes are crucial to elucidate the basic mechanisms of vibrationally coupled electron transport through a single-molecule contact, despite the fact that these processes do not directly contribute to the electrical current that is flowing through the junction.

Copyright line will be provided by the publisher

1 Introduction The study of single-molecule junctions represents a vibrant and challenging field of research comprising fundamentally important aspects of quantum and many-body physics as well as the possibility for technological applications in nanoelectronic devices [1]. Electron transport through a single-molecule junction can be understood in a similar way as through quantum dots, including electron-electron interactions [2] and/or quantum interference effects [3,4]. In addition, the vibrational degrees of freedom of a molecule play an important role [5, 6,4], including, in particular, nonequilibrium effects such as current-induced vibrational excitation [7, 8, 9, 10, 11, 12, 13, 14, 15, 16, 4, 17]. This is in contrast to quantum dot systems [18], where phonon degrees of freedom are often considered as being part of the environment rather than as

active degrees of freedom, and is associated to the small size and mass of a molecular conductor.

The key to understand this nonequilibrium transport problem is to account for all relevant processes. Quite intuitively, this includes transport processes, where an electron is transferred from one electrode to another. In the presence of an external bias voltage, these processes give rise to an electrical current that is flowing through the molecule. However, these are not the only processes that occur in single-molecule junctions. Considering the simpler setup of a molecule adsorbed on a surface, it is well known that electron-hole pair creation processes, where an electron transfers from the substrate onto the molecule and back, constitute the most important relaxation mechanism for vibrational excitation [19]. Such pair creation processes do also occur in single-molecule junctions, although their im-

Copyright line will be provided by the publisher

portance for the respective nonequilibrium transport properties has been established only recently [9,20,21,16,22,17,4]. In this article, we review the most important aspects of our work on this subject [20,21,16,22,23,17,4]. This includes a detailed understanding of the vibrational excitation characteristic, in particular the counter-intuitive phenomenon that larger levels of vibrational excitation are obtained for systems with weaker electronic-vibrational coupling [14,22]. In addition, pair creation processes may also have a substantial influence on the electrical transport properties of a single-molecule contact, giving rise, for example, to negative differential resistance, rectification [14] and important implications for spectroscopical applications of single-molecule junctions [23]. Pair creation processes can even facilitate a mechanism to control the excitation level of specific vibrational modes selectively via the external bias voltage [20,21] and, in the presence of destructive interference effects, of the electrical current via the temperature in the electrodes [22,17]. Note that the latter has been experimentally verified only recently [4].

The article is organized as follows. In Sec. 2, we introduce the model Hamiltonian and the nonequilibrium Green's function (NEGF) approach [24,25,10,21] that we use to describe electron transport through a single-molecule junction. Our results are presented in Sec. 3, where we set the stage by a discussion of the basic transport processes (Sec. 3.1) and electron-hole pair creation processes (Sec. 3.2), including a detailed analysis of the vibrational excitation characteristic of a generic molecular junction. Transport phenomena that are attributed to the influence of electron-hole pair creation processes are summarized in the last section, Sec. 3.3. Note that the presented data has already been published in Ref. [23].

2 Theory

2.1 Model Hamiltonian We consider a model for a molecular junction obtained by a partitioning of the overall system into the molecule and the left and right leads. The molecular part of a single-molecule junction (M) is often described by a set of discrete electronic states [7,1]. The Hamiltonian of the corresponding electronic degrees of freedom can be written as [14]

$$H_{\text{el}} = \sum_{m \in \text{M}} \epsilon_m c_m^\dagger c_m + \sum_{m < n \in \text{M}} U_{mn} (c_m^\dagger c_m - \delta_m)(c_n^\dagger c_n - \delta_n), \quad (1)$$

where ϵ_m denotes the energy of the m th molecular state and c_m^\dagger/c_m the corresponding creation/annihilation operators. Thereby, the index m distinguishes, in principle, different molecular orbitals, including the spin of the electrons. However, as the effects and mechanisms that are discussed in this review article do not explicitly involve spin degrees of freedom, we suppress them in the following. Coulomb interactions are described in the model

Hamiltonian H by Hubbard-like electron-electron interaction terms, $U_{mn}(c_m^\dagger c_m - \delta_m)(c_n^\dagger c_n - \delta_n)$. Thereby, we account for the fact that the single-particle energies ϵ_m are determined with respect to a specific reference state of the molecule (*e.g.*, the ground state of the uncharged molecule) [26,27] and that, effectively, these energies include Coulomb interactions between the electrons of the reference system. Therefore, we distinguish occupied ($\delta_m = 1$) and unoccupied states ($\delta_m = 0$) of the reference state to avoid double counting of electron-electron interactions.

Besides the electronic degrees of freedom, nuclear motion and/or electronic-vibrational coupling plays a key role in transport through molecular conductors [7,10,28,5,4], which is associated with their small size and mass. We take into account the vibrational degrees of freedom of a molecular conductor as harmonic oscillators that are linearly coupled to the electron (or hole) densities ($c_m^\dagger c_m - \delta_m$) [26,27],

$$H_{\text{vib}} = \sum_{\alpha} \Omega_{\alpha} a_{\alpha}^{\dagger} a_{\alpha} + \sum_{m\alpha} \lambda_{m\alpha} Q_{\alpha} (c_m^{\dagger} c_m - \delta_m), \quad (2)$$

where the operator a_{α}^{\dagger} denotes the creation operator of the α th oscillator with frequency Ω_{α} and $Q_{\alpha} = a_{\alpha} + a_{\alpha}^{\dagger}$ the corresponding vibrational displacement operators. The respective coupling strengths are denoted by $\lambda_{m\alpha}$. Note that we identify the vibrational degrees of freedom of the junction as the normal modes of the aforementioned reference state. As a consequence, electronic-vibrational coupling is required to vanish for that state, which, similarly as for the electron-electron interaction terms, is ensured by the parameters δ_m .

In most experiments on single-molecule junctions the molecule is contacted by metal electrodes. Accordingly, we describe the left (L) / right (R) electrode by a continuum of non-interacting electronic states

$$H_{\text{L/R}} = \sum_{k \in \text{L/R}} \epsilon_k c_k^{\dagger} c_k \quad (3)$$

that are localized in the left/right lead. The coupling between the molecule and the leads is given by

$$H_{\text{tun}} = \sum_{k \in \text{L,R}; m \in \text{M}} (V_{mk} c_k^{\dagger} c_m + \text{h.c.}), \quad (4)$$

where the coupling matrix elements V_{mk} determine the so-called level-width functions

$$\Gamma_{K,mn}(\epsilon) = 2\pi \sum_{k \in K} V_{mk}^* V_{nk} \delta(\epsilon - \epsilon_k) \quad (5)$$

with $K \in \{\text{L}, \text{r}\}$. Throughout this work, we assume semi-infinite tight-binding chains as models for the leads with an internal hopping parameter $\gamma = 2\text{eV}$. The corresponding level-width functions are given by [29]

$$\Gamma_{K,mn}(\epsilon) = \frac{\nu_{K,m} \nu_{K,n}}{\gamma^2} \sqrt{4\gamma^2 - (\epsilon - \mu_K)^2}, \quad (6)$$

where, similar to V_{mk} , the parameters $\nu_{K,m}$ denote the coupling strength of state m to lead K . In addition, we assume a symmetric drop of the bias voltage Φ at the contacts, *i.e.* the chemical potentials in the left and the right lead are given by $\mu_L = e\Phi/2$ and $\mu_R = -e\Phi/2$, respectively. Furthermore, we set the Fermi energy of the leads to $\epsilon_F = 0$ eV. The Hamiltonian of the overall system is thus given by the sum

$$H = H_{\text{el}} + H_{\text{vib}} + H_L + H_R + H_{\text{tun}}. \quad (7)$$

For the NEGF approach that we introduce in Sec. 2.2, it is expedient to remove the direct electronic-vibrational coupling terms in the Hamiltonian H by the small polaron transformation [30,24]:

$$\begin{aligned} \bar{H} = e^S H e^{-S} = & \sum_m \bar{\epsilon}_m c_m^\dagger c_m + \sum_\alpha \Omega_\alpha a_\alpha^\dagger a_\alpha \quad (8) \\ & + \sum_{m < n} \bar{U}_{mn} (c_m^\dagger c_m - \delta_m)(c_n^\dagger c_n - \delta_n), \\ & + \sum_{km} (V_{mk} X_m c_k^\dagger c_m + \text{h.c.}) + \sum_k \epsilon_k c_k^\dagger c_k, \end{aligned}$$

with

$$S = -i \sum_{m\alpha} (\lambda_{m\alpha} / \Omega_\alpha) (c_m^\dagger c_m - \delta_m) P_\alpha, \quad (9)$$

$$X_m = \exp[i \sum_\alpha (\lambda_{m\alpha} / \Omega_\alpha) P_\alpha], \quad (10)$$

and $P_\alpha = -i(a_\alpha - a_\alpha^\dagger)$. The effect of electronic-vibrational coupling is thus subsumed in a renormalization of the single-particle energies, $\bar{\epsilon}_m = \epsilon_m + (2\delta_m - 1) \sum_\alpha (\lambda_{m\alpha}^2 / \Omega_\alpha)$, the electron-electron interaction strengths, $\bar{U}_{mn} = U_{mn} - 2 \sum_\alpha (\lambda_{m\alpha} \lambda_{n\alpha} / \Omega_\alpha)$, and the molecule-lead coupling strengths that are dressed by the shift-operators X_m .

2.2 Nonequilibrium Green's Function Approach

All single-particle observables, such as, *e.g.*, the population of levels or the electrical current that is flowing through the junction, can be calculated from the single-particle Green's functions of the system. For the electronic degrees of freedom of our present problem, they are given by

$$\begin{aligned} G_{mn}(\tau, \tau') = & -i \langle T_c c_m(\tau) c_n^\dagger(\tau') \rangle_H \quad (11) \\ = & -i \langle T_c c_m(\tau) X_m(\tau) c_n^\dagger(\tau') X_n^\dagger(\tau') \rangle_{\bar{H}}. \end{aligned}$$

where the indices H/\bar{H} indicate the Hamiltonian that is used to evaluate the respective expectation values. We employ the ansatz [24,25,10,21]:

$$G_{mn}(\tau, \tau') \approx \bar{G}_{mn}(\tau, \tau') \langle T_c X_m(\tau) X_n^\dagger(\tau') \rangle_{\bar{H}}, \quad (12)$$

to calculate these Green's functions with $\bar{G}_{mn}(\tau, \tau') = -i \langle T_c c_m(\tau) c_n^\dagger(\tau') \rangle_{\bar{H}}$ and T_c the time-ordering operator on the Keldysh contour. The ansatz (12) represents an effective factorization of the single-particle Green's functions G_{mn} into a product of the electronic Green's functions, \bar{G}_{mn} , and a correlation function of shift operators, $\langle T_c X_m(\tau) X_n^\dagger(\tau') \rangle_{\bar{H}}$. This is justified, if the time scales

for electronic processes and vibrational motion in the junction are different, and is conceptually similar to the Born-Oppenheimer approximation [31].

We use an equation of motion technique to determine the single-particle Green's functions of the present problem [24,25,10,21]. The equation of motion for the electronic part of the Green's function reads

$$\begin{aligned} (i\partial_\tau - \bar{\epsilon}_m) \bar{G}_{mn}(\tau, \tau') (-i\partial_{\tau'} - \bar{\epsilon}_n) = & \quad (13) \\ \delta(\tau, \tau') \delta_{mn} (-i\partial_{\tau'} - \bar{\epsilon}_n) & \\ + \Sigma_{\text{Coul},mn}(\tau, \tau') + \sum_{K \in \{L,R\}} \Sigma_{K,mn}(\tau, \tau'), & \end{aligned}$$

where the self-energy contributions due to the coupling of the molecule to the left and the right leads are given by

$$\begin{aligned} \Sigma_{L/R,mn}(\tau, \tau') = & \quad (14) \\ \sum_{k \in L/R} V_{mk}^* V_{nk} g_k(\tau, \tau') \langle T_c X_n(\tau') X_m^\dagger(\tau) \rangle_{\bar{H}} \end{aligned}$$

with $g_k(\tau, \tau')$ the free Green's function associated with lead state k . The effect of electron-electron interactions is subsumed in the self-energy $\Sigma_{\text{Coul},mn}(\tau, \tau')$. We describe the latter in terms of the elastic co-tunneling approximation [32,33,10,21], where $\Sigma_{\text{Coul},mn}(\tau, \tau')$ is replaced by the self-energy $\Sigma_{\text{Coul},mn}^0(\tau, \tau')$ describing electron-electron interactions in the isolated molecule (*i.e.* where $V_{mk} = 0$), facilitating a nonperturbative description of electron-electron interactions.

The correlation functions of the shift operators, $\langle T_c X_m(\tau) X_n^\dagger(\tau') \rangle_{\bar{H}}$, which represent the second part of the factorized Green's function \bar{G}_{mn} (cf. Eq. (12)), can be determined employing a second-order cumulant expansion in the dimensionless coupling parameters $\frac{\lambda_{m\alpha}}{\Omega_\alpha}$ [10,21]

$$\begin{aligned} \langle T_c X_m(\tau) X_n^\dagger(\tau') \rangle_{\bar{H}} = & \quad (15) \\ e^{\sum_{\alpha\alpha'} i \frac{\lambda_{m\alpha} \lambda_{n\alpha'}}{\Omega_\alpha \Omega_{\alpha'}} D_{\alpha\alpha'}(\tau, \tau') - i \frac{\lambda_{m\alpha} \lambda_{m\alpha'} + \lambda_{n\alpha} \lambda_{n\alpha'}}{2\Omega_\alpha \Omega_{\alpha'}} D_{\alpha\alpha'}(\tau, \tau)}, \end{aligned}$$

with the momentum correlation functions

$$D_{\alpha\alpha'} = -i \langle T_c P_\alpha(\tau) P_{\alpha'}(\tau') \rangle_{\bar{H}}. \quad (16)$$

These single-particle Green's functions can also be determined evaluating their equations of motion

$$\begin{aligned} \frac{1}{4\Omega_\alpha \Omega_{\alpha'}} (-\partial_\tau^2 - \Omega_\alpha^2) D_{\alpha\alpha'}(\tau, \tau') (-\partial_{\tau'}^2 - \Omega_{\alpha'}^2) = & \quad (17) \\ \delta(\tau, \tau') \delta_{\alpha\alpha'} (-\partial_{\tau'}^2 - \Omega_{\alpha'}^2) \frac{1}{2\Omega_{\alpha'}} + \Pi_{\text{el},\alpha\alpha'}(\tau, \tau'). \end{aligned}$$

The corresponding self-energy matrix $\Pi_{\text{el},\alpha\alpha'}$ is evaluated up to second order in the molecule-lead coupling [10,21]

$$\begin{aligned} \Pi_{\text{el},\alpha\alpha'}(\tau, \tau') = & -i \sum_{mn} \frac{\lambda_{m\alpha} \lambda_{n\alpha'}}{\Omega_\alpha \Omega_{\alpha'}} \times \quad (18) \\ (\Sigma_{mn}(\tau, \tau') \bar{G}_{nm}(\tau', \tau) + \Sigma_{nm}(\tau', \tau) \bar{G}_{mn}(\tau, \tau')). \end{aligned}$$

Since $\Pi_{\text{el},\alpha\alpha'}$ depends on the electronic self-energies $\Sigma_{mn} = \Sigma_{L,mn} + \Sigma_{R,mn}$ and Green's functions \bar{G}_{mn} , the evaluation of Eqs. (13) and (17) requires an iterative self-consistent solution scheme [10,21].

2.3 Observables of interest To characterize electron transport through a single-molecule junction, we analyze two different observables of interest as functions of the applied bias voltage Φ : the average vibrational excitation and the electrical current flowing through the junction. The average level of excitation of vibrational mode α is given by

$$\langle a_\alpha^\dagger a_\alpha \rangle_H = \langle a_\alpha^\dagger a_\alpha \rangle_{\overline{H}} + \sum_{mn} \frac{\lambda_{m\alpha} \lambda_{n\alpha}}{\Omega_\alpha^2} \langle (c_m^\dagger c_m - \delta_m)(c_n^\dagger c_n - \delta_n) \rangle_{\overline{H}}. \quad (19)$$

where the latter terms represent the contribution from polaron-formation, which is associated with charging of the molecular bridge. It can be computed from the vibrational Green's function $D_{\alpha\alpha}$ according to [21]

$$\begin{aligned} \langle a_\alpha^\dagger a_\alpha \rangle_H &\approx -\frac{1}{2} \text{Im} [D_{\alpha\alpha}^<(t=0)] - \frac{1}{2} \\ &+ \sum_m \frac{\lambda_{m\alpha}^2}{\Omega_\alpha^2} (\text{Im}[\overline{G}_{mm}^<(t=0)] - \delta_m) \\ &- 2 \sum_{m<n} \frac{\lambda_{m\alpha} \lambda_{n\alpha}}{\Omega_\alpha^2} (\text{Im}[\overline{G}_{mn}^<(t=0)] \text{Im}[\overline{G}_{nm}^<(t=0)] \\ &- \text{Im}[\overline{G}_{mm}^<(t=0)] - \delta_m) (\text{Im}[\overline{G}_{nn}^<(t=0)] - \delta_n), \end{aligned} \quad (20)$$

where the electronic Green's function \overline{G}_{mn} and the Hartree-Fock-like factorization

$$\langle c_m^\dagger c_m c_n^\dagger c_n \rangle_{\overline{H}} \approx \langle c_m^\dagger c_m \rangle_{\overline{H}} \langle c_n^\dagger c_n \rangle_{\overline{H}} - \langle c_m^\dagger c_n \rangle_{\overline{H}} \langle c_n^\dagger c_m \rangle_{\overline{H}} \quad (21)$$

for $m \neq n$ is used to represent the contribution from polaron-formation.

The current through lead K , I_K , is determined by the number of electrons entering or leaving the lead in a given time interval ($K \in \{L, R\}$)

$$I_K = -2e \frac{d}{dt} \sum_{k \in K} \langle c_k^\dagger c_k \rangle_{\overline{H}}. \quad (22)$$

Here, the constant ($-e$) denotes the electron charge and the factor 2 accounts for spin-degeneracy. With the self-energies $\Sigma_{L,R,mn}$ and Green's functions G_{mn} (cf. Sec. 2.2), the current can be calculated employing the Meir-Wingreen-like formula [34, 25, 10]

$$I_K = 2e \int \frac{d\epsilon}{2\pi} \sum_{mn} (\Sigma_{K,mn}^<(\epsilon) \overline{G}_{nm}^>(\epsilon) - \Sigma_{K,mn}^>(\epsilon) \overline{G}_{nm}^<(\epsilon)). \quad (23)$$

Note that the NEGF approach is current conserving, *i.e.* $I_L = -I_R = I$.

2.4 Vibrations in thermal equilibrium In addition to the nonequilibrium treatment discussed above, we also employ a simpler 'equilibrium' description, where we neglect the vibrational self-energy, *i.e.* $\Pi_{\text{el},\alpha\alpha'}(t, t') = 0$. This is a commonly used approximation [30, 24, 25, 14] and constitutes a powerful tool to elucidate and analyze nonequilibrium effects. Within this approximation, the vibrational degrees of the junction are effectively confined to

model	ϵ_1	$\nu_{L,1}$	$\nu_{R,1}$	γ	Ω_1	λ_{11}
EIV1	0.6	0.1	0.1	3	0.1	0.06
BAND	0.15	0.02	0.02	0.2	0.1	0.06
REC	0.6	0.1	0.03	3	0.1	0.06
RECBD	0.15	0.02	0.006	0.2	0.1	0.06

Table 1 Model parameters for molecular junctions with a single electronic state (energy values are given in eV). The temperature in the leads is assumed to be $T = 10$ K throughout the article. Note that the parameters of all the model systems that we discuss in this review article fulfill the antiadiabatic condition $\Gamma_{L,R,11} < \Omega_1$ and that they are in line with previous experimental [36, 37, 38, 39, 40, 28, 41, 5, 4] and theoretical findings [42, 43, 27, 44, 45, 46].

the state they would acquire in thermal equilibrium at an effective temperature $k_B T$. This means that, in contrast to a full nonequilibrium calculation, tunneling electrons may, indeed, excite or deexcite the vibrational degrees of freedom of the junction but that such changes of the vibrational state decay instantly such that an electron that is tunneling subsequently through the junction finds the vibrational mode in the same equilibrium state as before.

3 Results We study the importance of resonant electron-hole pair creation processes for vibrationally coupled electron transport in single-molecule junctions in three steps of increasing complexity. First, in Sec. 3.1, we introduce the basic transport processes and mechanisms that occur in the resonant transport regime of a molecular junction. To this end, we discuss the current-voltage characteristics of two generic model systems of molecular junctions that include a single and two electronic states. This provides the basis for our discussion in Sec. 3.2, where we introduce electron-hole pair creation processes on the very same grounds as transport processes. Thereby, we analyze the vibrational excitation characteristics of the model systems that we already discussed in Sec. 3.1. It is shown that electron-hole pair creation processes are crucial to understand the (current-induced) levels of vibrational excitation in a single-molecule junction, including the respective electrical transport properties. This is exemplified in more detail in Sec. 3.3, where we discuss various transport phenomena that can be traced back to the influence of electron-hole pair creation processes. Note that the validity of the results, which are presented in the following and based on the NEGF scheme outlined in Sec. 2.2, have been corroborated by comparison to Born-Markov master equation approaches [10, 21, 23] and a numerically exact wave-propagation scheme [35].

3.1 Basic transport processes To discuss the basic transport processes that occur in single-molecule junctions, we consider first a simple model for a molecular junction with a single electronic state that is coupled to a single vibrational mode (model EIV1, see Tab. 1 for a

model	ϵ_1	ϵ_2	U_{12}	$\nu_{L,1}$	$\nu_{L,2}$	$\nu_{R,1}$	$\nu_{R,2}$	γ	Ω_1	Ω_2	λ_{11}	λ_{21}	λ_{12}	λ_{22}
E2V1	0.15	0.8	0	0.1	0.1	0.1	0.1	3	0.1	–	0.06	-0.06	–	–
SPEC	0.15	0.8	0	0.1	0.1	0.03	0.03	3	0.1	–	0.06	-0.06	–	–
MSVE	0.65	-0.575	0	0.1	0.1	0.03	0.03	2	0.15	0.2	0.09	0	0	0.12
INT	0.5123	0.5126	0.0248	0.01	0.01	0.01	-0.01	0.25	0.005	–	0.0248	0.025	–	–

Table 2 Model parameters for molecular junctions with two electronic states (energy values are given in eV).

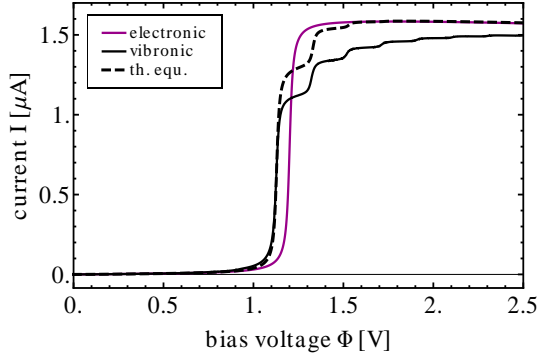


Figure 1 Current-voltage characteristics of junction E1V1 (cf. Tab. 1 for the corresponding model parameters).

detailed list of all model parameters). The corresponding current-voltage characteristic is shown in Fig. 1, where we distinguish three different scenarios: *i*) the electronic scenario (solid purple line), where we neglect the effect of electronic-vibrational coupling, *ii*) the vibronic scenario (solid black line), where we fully account for the coupling between the electronic state and the vibration, and *iii*) the thermally equilibrated scenario (dashed black line), where electronic-vibrational is accounted for but the vibration is restricted to the state it acquires in thermal equilibrium at $T = 10$ K (which is effectively its ground state).

Within the electronic scenario, the current-voltage characteristic displays a single step at $e\Phi = 2\epsilon_1$, which is associated with the onset of resonant electronic transport processes where electrons are tunneling through the junction in two subsequent resonant tunneling events (see Fig. 2a). In contrast, the vibronic scenarios provide a number of additional resonant transport channels that become active at different bias voltages [14]. Some of them are readily active at the onset of the resonant transport regime at $e\Phi = 2\bar{\epsilon}_1$ and include both resonant excitation (Fig. 2b) and resonant deexcitation processes (Fig. 2c). Another set of resonant excitation processes (Fig. 2d) becomes active at higher bias voltages, $e\Phi = 2(\bar{\epsilon}_1 + n\Omega_1)$ ($n \in \mathbb{N}$), giving rise to additional steps in the vibronic current-voltage characteristics.

The height of the steps in the current-voltage characteristics is different for all three transport scenarios, reflecting

the fact that the corresponding transport processes strongly depend on the electronic-vibrational coupling strength λ_{11} and the vibrational excitation level of the junction. The respective probabilities can be expressed in terms of the so-called Franck-Condon matrix elements F_{mn} , that is the transition matrix elements from the m th to the n th state of the vibrational mode upon change of the charge state of the molecule. If, for example, electronic transport processes (Fig. 2a) occur with a relative probability of 1 in the electronic scenario, they occur with a reduced probability of $F_{00} \approx 0.7$ in the thermally equilibrated transport scenario. This value becomes even smaller in the vibronic transport scenario, $\sum_n p_n F_{nn} < F_{00}$, where p_n represents the average population of the n th vibrational level. The first step in the current-voltage characteristics at $e\Phi = 2\bar{\epsilon}_1$ is correlated with these probabilities, although a quantitative analysis is much more involved [14]. The subsequent steps at $e\Phi = 2(\bar{\epsilon}_1 + n\Omega_1)$ become successively smaller, which can be qualitatively understood by the reduced Franck-Condon matrix elements of the respective transport processes that involve transitions from the vibrational ground state to the n th excited state of the vibration, $F_{0n} = e^{-\lambda_{11}^2/\Omega_1^2} (\lambda_{11}^{2n}/\Omega_1^{2n})/n!$. However, as the comparison of the dashed black and the solid black line shows, vibrational nonequilibrium effects significantly modify the step structure and lead, in general, to a suppression of the electrical current that is flowing through junction E1V1 [14].

So far, we have considered transport processes for a model with a single electronic state. In many cases, however, electron transport through single-molecule junctions is carried by a multitude of states. The resulting vibrational processes that may occur with respect to each of these states leads to a number of interesting (nonequilibrium) phenomena (see, e.g., Refs. [10, 11, 13, 14, 17]). As an example, we consider a junction with two electronic states (model E2V1, see Tab. 2 for a complete list of parameters). The corresponding current-voltage characteristics are shown in Fig. 3.

The current-voltage characteristic associated with the electronic scenario shows two steps at $e\Phi = 2\epsilon_1 = 0.3$ eV and $e\Phi = 2\epsilon_2 = 1.6$ eV, indicating the onset of electronic transport processes through states 1 and 2, respectively. Similarly, the thermally equilibrated transport shows three pronounced steps at $e\Phi = 2\bar{\epsilon}_1 = 0.228$ eV, $e\Phi = 2\bar{\epsilon}_2 = 1.528$ eV and $e\Phi = 2(\bar{\epsilon}_2 + \bar{U}_{12}) = 1.672$ eV, where the first of these steps is, just as in the electronic scenario,

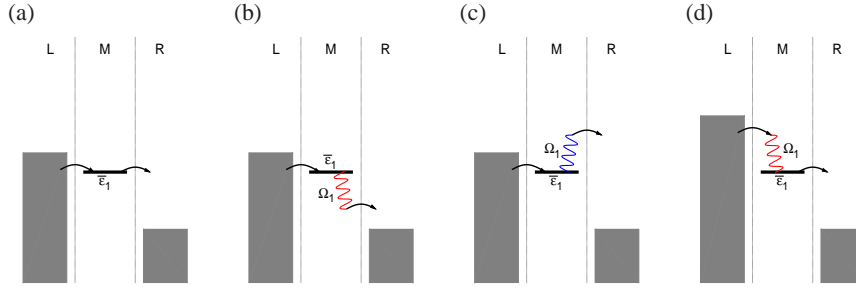


Figure 2 Schematic representation of example processes for sequential tunneling in a molecular junction. Panel (a) shows sequential tunneling of an electron from the left lead to the right lead that involves two consecutive tunneling processes: from the left lead onto the molecular bridge and from the molecular bridge to the right lead. In panel (b)/(c) the latter of the two tunneling processes is accompanied by an excitation/deexcitation process, where due to electronic-vibrational coupling the vibrational mode is singly excited/deexcited. While the processes depicted by Panel (a) – (c) become active at the same bias voltage, that is for $e\Phi \approx 2\bar{\epsilon}_1$, resonant excitation processes like the one depicted by Panel (d) require higher bias voltages, $e\Phi \gtrsim 2\bar{\epsilon}_1 + \Omega_1$.

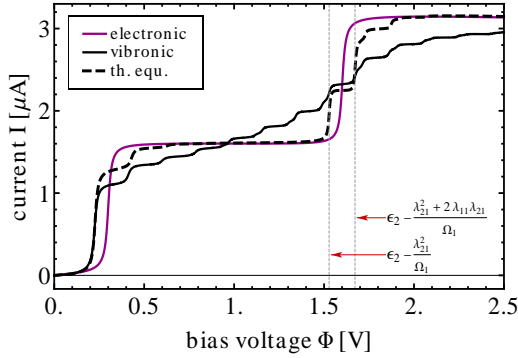


Figure 3 Current-voltage characteristics of junction E2V1 (cf. Tab. 2).

associated with the onset of resonant electronic transport processes through the first electronic level. The other two steps originate from the onset of resonant electronic transport processes through the second electronic level. However, due to electron-electron interactions, $\bar{U}_{12} = 72$ meV, transport through this state depends on whether the first level is occupied or unoccupied. This leads to a splitting of the corresponding step into two steps that are separated by $e\Delta\Phi = 2\bar{U}_{12}$. Apart from the splitting of steps due to electron-electron interactions, the current-voltage characteristics of the thermally equilibrated scenario can be understood on the same grounds as for a junction with a single electronic level. Vibrational side-steps are observed with respect to each of the three electronic resonances, that is at $e\Phi = 2(\bar{\epsilon}_1 + n\Omega_1)$, $e\Phi = 2(\bar{\epsilon}_2 + n\Omega_1)$ and $e\Phi = 2(\bar{\epsilon}_2 + \bar{U}_{12} + n\Omega_1)$ ($n \in \mathbb{N}$). They indicate, as before, the onset of resonant excitation processes (see Figs. 2d and 4a). This shows that the onset of vibrational pro-

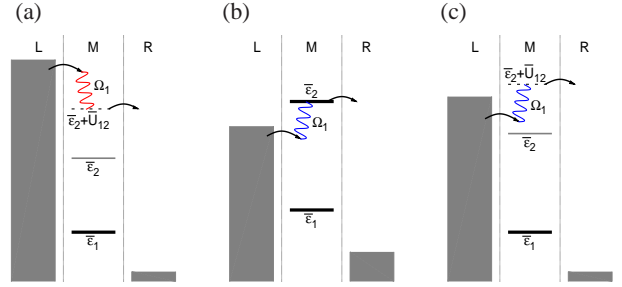


Figure 4 Examples of sequential tunneling processes involving two electronic states. Panel (a) depicts a sequential tunneling process, which involves an excitation processes with respect to state 2. Thereby, it is assumed that state 1 is occupied, that is the tunneling electron requires an energy of $\epsilon_2 + U_{12} + \Omega_1$, which is increased by the charging energy U_{12} due to interaction with the electron in state 1. Panels (c) and (d) show corresponding deexcitation processes, where the lower-lying electronic state is unoccupied and occupied, respectively.

cesses does not only depend on the position of the electronic levels, given by $\bar{\epsilon}_m$, but also on the electron-electron interaction strengths \bar{U}_{mn} .

In contrast, the vibronic scenario shows a more complex behavior. For example, it exhibits only a single pronounced step at $e\Phi = 2\bar{\epsilon}_1$. The two steps associated with the onset of resonant transport through the second electronic state are barely visible. This is due to the current-induced level of vibrational excitation, which is generated by inelastic processes with respect to the first state (Fig. 2d). This leads, on one hand, to a reorganization of the steps heights and an overall reduction of the current level through state 1 (cf. the discussion of Fig. 1 or see Ref. [14]

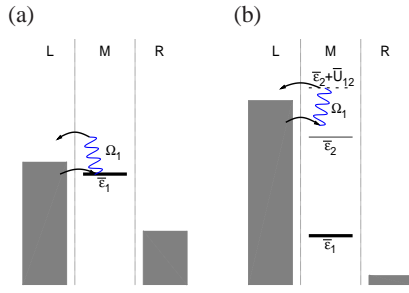


Figure 5 Examples of electron-hole pair creation processes. Panel (a) shows a resonant electron-hole pair creation process, where in two sequential tunneling events an electron tunnels from the left lead onto the molecular bridge and back again to the left lead. Thereby, the electron takes up a quantum of vibrational energy (blue wiggly line). A pair creation process with respect to a higher-lying electronic state is shown in Panel (b).

for a more detailed analysis of these phenomena). On the other hand, it triggers resonant deexcitation processes with respect to the second electronic state (Figs. 4b and 4c) even before it has entered the bias window [10, 14]. As a result, the steps corresponding to transport through state 2 are effectively broadened such that, instead of two pronounced steps, the onset of resonant transport through the second electronic state is associated with a number of small steps at $e\Phi = 2(\bar{\epsilon}_2 - n\Omega_1)$ and $e\Phi = 2(\bar{\epsilon}_2 + \bar{U}_{12} - n\Omega_1)$ [10]. This shows that vibrational nonequilibrium effects have a pronounced influence on the electrical transport properties of a molecular junction and that a more detailed and quantitative understanding of these effects requires an analysis of the corresponding vibrational excitation characteristic (which will be given in Sec. 3.2).

3.2 Electron-hole pair creation processes In this section, we analyze the vibrational excitation characteristics of junctions E1V1 and E2V2. This requires to account for all processes, where the molecule exchanges energy with the electrodes, including inelastic transport processes (see Figs. 2 and 4) as well as electron-hole pair creation processes (examples of which are depicted in Fig. 5). Pair creation and transport processes involve the same tunneling processes and, therefore, occur principally with the same probability. They are distinguished only by the fact that the tunneling electrons return to the same lead in the course of a pair creation event, while they transfer from one lead to the other in the course of a transport process.

The excitation characteristics of junction E1V1 is depicted by the solid black line in Fig. 6. It shows a qualitatively different behavior with respect to the applied bias voltage Φ than the corresponding current-voltage characteristics (cf. Sec. 3.1). Although it exhibits steps at the same bias voltages, the height of these steps follows clearly another phenomenology. While the steps in the current-

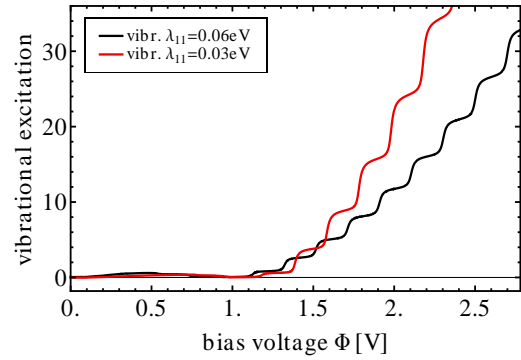


Figure 6 Vibrational excitation characteristic of junction E1V1 (cf. Tab. 1).

voltage characteristic become successively smaller with an increasing bias voltage Φ , they become successively larger in the vibrational excitation characteristic. Thus, in contrast to the current-voltage characteristics, the level of vibrational excitation does not saturate for high bias voltages [22]. Moreover, the step heights increase if the electronic-vibrational coupling strength is reduced. This can be inferred from the comparison of the vibrational excitation characteristic of junction E1V1 with the excitation characteristic of a very similar junction that differs from junction E1V1 only by a reduced electronic-vibrational coupling strength $\lambda_{11} = 0.03$ eV. It is depicted by the solid red line in Fig. 6. This behavior is rather counter-intuitive, because the transition matrix elements for the corresponding excitation processes (Fig. 2d) become smaller for weaker electronic-vibrational coupling strengths λ_{11} [30, 47, 48, 14, 22].

To understand the phenomenology of the vibrational excitation characteristics it is expedient to consider the nature of this observable. In contrast to the electrical current, which is determined by the number of transport processes in a given time interval, the level of vibrational excitation (in steady state) is determined by the ratio of the probabilities for excitation and deexcitation processes. At low bias voltages, $e\Phi \lesssim 2\bar{\epsilon}_1$, vibrational excitation can only be generated in tunneling processes with respect to the right lead (cf. Fig. 2b). Resonant deexcitation, however, is less restricted and can occur with respect to both leads (e.g. by the processes that are depicted in Figs. 2c and 5a). This leads, roughly speaking, to a ratio between the probabilities for excitation and deexcitation of the vibrational mode of at least one to two. The corresponding level of vibrational excitation is, therefore, rather low and originates, to a large extent, from polaron formation (see Eqs. (19) and (20)). At higher bias voltages $e\Phi > 2(\bar{\epsilon}_1 + \Omega_1)$, however, the imbalance between excitation and deexcitation processes becomes gradually smaller. This is, on one hand, due to an increasing number of excitation processes that become ac-

tive but, on the other hand, also due to a decreasing number of deexcitation processes that were active at smaller bias voltages. For example, the electron-hole pair creation process depicted in Fig. 5a is active at the onset of the resonant transport regime but is blocked for bias voltages $e\Phi > 2(\bar{\epsilon}_1 + \Omega_1)$. Thus, the probabilities for excitation and deexcitation of the vibrational mode become successively the same, resulting in an indefinite increase of vibrational excitation at higher bias voltages, where only transport processes occur [22]. Moreover, as the pair-creation processes that are blocked at $e\Phi > 2(\bar{\epsilon}_1 + n\Omega_1)$ are more important for weaker electronic-vibrational coupling, the corresponding increase/step in the vibrational excitation characteristic becomes larger for smaller values of λ_{11} [14, 22].

Similar as in Sec. 3.1, we extend our considerations at this point to a junction with two electronic states, model E2V1. The vibrational excitation characteristic of this junction is shown in Fig. 7. As long as the second electronic state is located far outside the bias window (for $\Phi \lesssim 1$ V), the level of vibrational excitation increases monotonously due to resonant excitation processes with respect to the first electronic state (Fig. 2d). At higher bias voltages, however, the vibrational energy thus generated facilitates resonant deexcitation processes with respect to the second electronic state, including transport (Figs. 4b and 4c) as well as electron-hole pair creation processes (Figs. 5b). These processes significantly reduce the level of vibrational excitation before the second electronic state enters the bias window (*i.e.* $1\text{ eV} < e\Phi < 2\bar{\epsilon}_2$). The net effect is that the presence of the second electronic state results in a cooling of the junction at these bias voltages [10, 14].

This cooling extends to even higher bias voltages, if electron-electron interactions are present. This can be seen by comparison of the solid black line in Fig. 7 with the solid blue line, which shows the vibrational excitation characteristic of a junction that differs from junction E2V1 only by additional repulsive electron-electron interactions, $U_{12} = 0.5\text{ eV}$. Due to the more pronounced splitting of the resonances that are associated with the second electronic state in this system, deexcitation processes due to both transport (Fig. 4c) and electron-hole pair creation processes (Fig. 5b) are shifted to higher energies and, consequently, become active at higher bias voltages. Thus, the additional electron-electron interactions lead to a slight increase of the level of vibrational excitation at low bias voltages (*i.e.* for $\Phi \lesssim 2$ V). At higher bias voltages, however, they lead to a significant decrease of the vibrational excitation level (Coulomb Cooling) [14].

3.3 Transport phenomena due to electron-hole pair creation processes The results discussed in the preceding section, Sec. 3.2, show that a detailed understanding of the vibrational excitation characteristic of a single-molecule contact can only be obtained if electron-hole pair creation processes are taken into account. Thus, pair creation processes also influence the corresponding

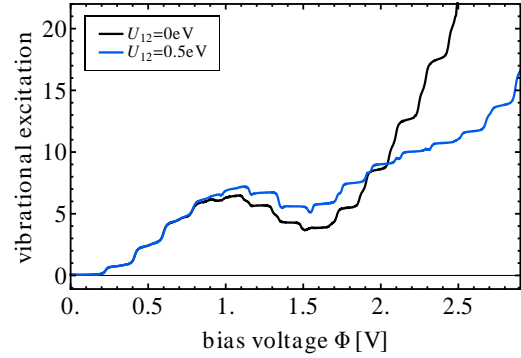


Figure 7 Vibrational excitation characteristics for junction E2V1 (solid black line, cf. Tab. 2). In addition, the vibrational excitation characteristics of a very similar system is shown, which, in contrast to junction E2V1, includes additional repulsive electron-electron interactions, $U_{12} = 0.5\text{ eV}$ (solid blue line).

electrical transport properties, as the efficiency of transport processes is strongly interrelated with the vibrational excitation levels (*cf.*, *e.g.*, the reduced current level in the resonant transport regime of junctions E1V1 and E1V2 discussed in Sec. 3.1). In this section, we show that this influence may be substantial and that it can lead to a number of interesting transport phenomena such as, for example, negative differential resistance (Sec. 3.3.1), rectification (Sec. 3.3.2), mode-selective vibrational excitation (Sec. 3.3.3) or a pronounced temperature dependence of the current in the presence of destructive quantum interference effects (Sec. 3.3.4).

3.3.1 Negative differential resistance In general, an electronic device exhibits negative differential resistance (NDR) when its differential conductance $dI/d\Phi$ becomes negative. This phenomenon is relevant for a number of applications in electronics, for example, in analog-digital converters [49] or logic circuits [50, 51]. A prime example for a nanoelectronic device that exhibits NDR is the resonant tunneling diode, where the overlap of the (narrow) conduction bands in the leads decreases with increasing bias voltage Φ [52, 53]. The current-voltage characteristic of a corresponding model for a molecular junction (model BAND, cf. Tab. 1) is depicted by the solid purple line in Fig. 8. At low bias voltages, where the conduction bands overlap with each other, the current level of the junction increases, in particular when resonant transport processes through the electronic state become active at $e\Phi \approx 2\epsilon_1$. At higher bias voltage, however, the overlap of the conduction bands continuously decreases such that electronic transport processes (Fig. 2a) can no longer connect an occupied state in one of the leads with an unoccupied state in the other lead. Thus, the current level of the junction decreases.

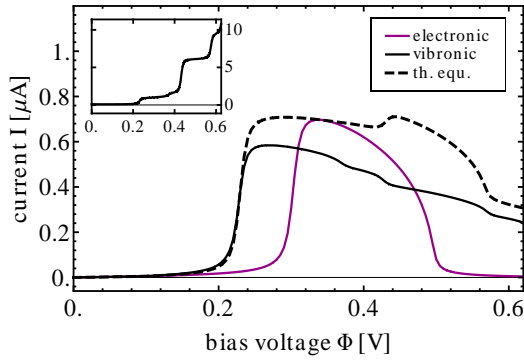


Figure 8 Current-voltage characteristics of a molecular junction that exhibits negative differential resistance (model BAND, cf. Tab. 1). The inset shows the corresponding vibrational excitation characteristic.

In the presence of electronic-vibrational coupling, the effect of the narrow conduction bands is significantly reduced, as can be seen by the solid black line in Fig. 8. This is due to inelastic transport processes, which allow electrons to span a much wider range of energies in the course of a transport process, increasing effectively the overlap of the conduction bands. In addition, however, another much more narrow NDR feature occurs at $e\Phi = 2(\bar{\epsilon}_1 + \Omega_1)$. It is in line with an increase of the vibrational excitation level of the junction (depicted in the inset of Fig. 8). The thermally equilibrated scenario (dashed black line), however, does not exhibit NDR at this bias voltage. On the contrary, it displays an increase of the current level. Thus, we trace this NDR effect back to the suppression of electron-hole pair creation processes (Fig. 5a) and the associated increase in vibrational excitation rather than the opening of another inelastic channel (Fig. 2d), although both occur at the same bias voltage. Note that this NDR effect is not related to the narrow conduction bands of this model system and that it may be more pronounced if the molecule is asymmetrically coupled to the leads (see, for example, Refs. [54, 55, 14]).

3.3.2 Vibrational rectification and spectroscopy in molecular junctions Diode-like behavior represents another important device characteristic [37]. Such behavior is often associated with an asymmetric coupling of the molecule to the leads. But an asymmetry in the molecule-lead coupling is not sufficient [56], as is demonstrated by the solid purple line in Fig. 9. It shows the electronic current-voltage characteristics of junction E1V1 with a reduced coupling strength to the right lead (model REC, cf. Tab. 1). It is almost perfectly antisymmetric with respect to the polarity of the bias voltage, *i.e.* $I(\Phi) = -I(-\Phi)$. The origin of this behavior is twofold. First, transport processes involve the coupling to both leads and, therefore, cannot transfer an asymmetry in the coupling to the leads

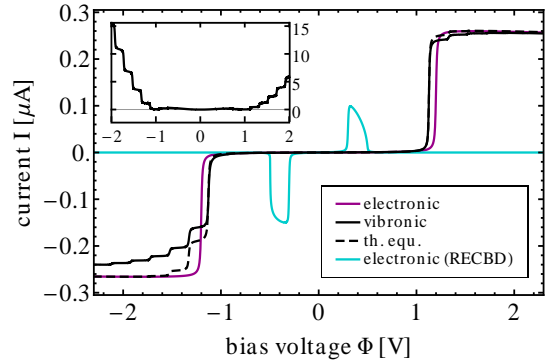


Figure 9 Current-voltage characteristics of the asymmetric junction REC (cf. Tab. 1). The inset shows the corresponding vibrational excitation characteristic. The solid turquoise line refers to model RECB (cf. Tab. 1), which is distinguished from junction REC in particular due to a much narrower band width γ .

to the transport characteristics of a molecular contact. Second, the density of states for these processes does also not display a pronounced asymmetry with respect to the bias voltage Φ . In particular in the limit $\nu_{R,1}/\nu_{L,1} \rightarrow 0$, where tunneling processes with respect to the right lead represent the bottleneck for transport, it is given by $\Gamma_{R,11}(\epsilon_1)/\nu_{R,1}^2$. If, however, in addition to an asymmetric molecule-lead coupling, the band width in the leads is reduced (from $\gamma = 3$ eV to $\gamma = 0.2$ eV), the density of states $\Gamma_{R,11}(\epsilon_1)/\nu_{R,1}^2$ is much smaller in the resonant transport regime for negative bias voltages ($e\Phi \lesssim 2\bar{\epsilon}_1$) than it is for positive bias voltages ($e\Phi \gtrsim 2\bar{\epsilon}_1$). In that case, the corresponding current-voltage characteristic exhibits an asymmetry with respect to the polarity of the applied bias voltage, which can be seen by the solid turquoise line in Fig. 9, which shows the current-voltage characteristic of such a junction (model RECB, cf. Tab. 1)¹.

Another mechanism that leads to a different current response at different polarities of the applied bias voltage is electronic-vibrational coupling [14, 21]. This can be seen by the solid black and dashed black lines in Fig. 9, which show the current-voltage characteristics of junction REC considering the vibronic and the thermally equilibrated transport scenario, respectively. While the black line exhibits a pronounced asymmetry of the current level, the dashed black line shows an asymmetry in the current level only in the vicinity $e\Phi \sim \pm 2\bar{\epsilon}_1$. For the thermally equilibrated scenario, this behavior can be deduced again from the density of states for resonant transport processes in the right lead. For positive bias voltages, $e\Phi \gtrsim 2\bar{\epsilon}_1$, it is given by $\sum_n F_{0n} \Gamma_{R,11}(\epsilon_1)/\nu_{R,1}^2 \approx \Gamma_{R,11}(\epsilon_1)/\nu_{R,1}^2$, where

¹ Note that for similar systems with $\epsilon_1 \approx 0$, the current response would be perfectly antisymmetric irrespective of an asymmetric molecule-lead coupling and the value of the band width γ .

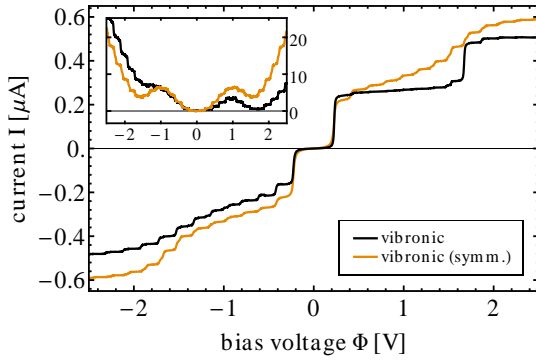


Figure 10 Current-voltage characteristics of the asymmetric junction SPEC (cf. Tab. 2). The inset shows the corresponding vibrational excitation characteristic. For comparison, the solid orange lines show results of the corresponding symmetric molecular junction E2V1 rescaled by a factor of $1/5$.

the sum over the Franck-Condon matrix elements F_{0n} indicates that electronic (Fig. 2a) as well as resonant excitation processes (Fig. 2b) become simultaneously active. For negative bias voltages, however, only electronic processes are active at $e\Phi = -2\bar{\epsilon}_1$, while excitation processes with respect to tunneling from the right lead become successively active at $e\Phi = -2(\bar{\epsilon}_1 + n\Omega_1)$. This leads to relative step heights in the current-voltage characteristics that are given by $F_{00}, F_{00} + F_{01}$, etc..

Although the same effects do also contribute to the asymmetric current response of the vibronic transport scenario, its behavior is strongly linked to the corresponding level of vibrational excitation (shown in the inset of Fig. 9). As the excitation levels of the junction are much higher for negative bias voltages, the current is more strongly suppressed than for positive bias voltages. This relation between high levels of vibrational excitation and a reduction of the current level has already been outlined in Sec. 3.1 (and in Refs. [14, 21]). As a consequence, the current suppression or the rectification effect also extends in the vibronic scenario over a wider range of bias voltages than for the thermally equilibrated scenario. Thereby, the asymmetry in vibrational excitation is due to electron-hole pair creation processes. In contrast to transport processes, they involve only one of the leads. Thus, in the limit $\nu_{R,1}/\nu_{L,1} \rightarrow 0$, electron-hole pair creation processes with respect to the left lead (Fig. 5a) are much more important than pair creation processes with respect to the right lead as well as excitation and deexcitation processes due to transport processes. Therefore, the vibrational mode is more efficiently cooled for positive than for negative bias voltages, since pair creation processes with respect to the left lead involve less vibrational quanta and, therefore, are more effective for positive than for negative bias voltages.

Considering spectroscopic applications of single-molecule junctions, the above described vibrational rectification effect leads to important implications. For example, one may observe a different number of side-steps (or different relative step heights) in the current-voltage characteristic of an asymmetrically coupled molecular junction by changing the polarity of the applied bias voltage (cf. Fig. 9) [5]. Furthermore, an asymmetry in the molecule-lead coupling may be useful to observe signals of states that are located further away from the Fermi level. According to our discussion of Fig. 3 (Sec. 3.1), these signals may be blurred by the effect of resonant deexcitation processes [10]. In asymmetric junctions, however, where the effect of local cooling by electron-hole pair creation processes is different for different bias polarities, these processes can be less pronounced, at least for one polarity of the applied bias voltage [23]. This is shown in Fig. 10, where the current-voltage characteristic of junction E2V1 is compared to a very similar junction that differs from junction E2V1 only by reduced coupling strengths to the right lead (model SPEC, cf. Tab. 1). In contrast to the symmetric junction E2V1, junction SPEC exhibits, due to the effect of a more pronounced cooling by electron-hole pair creation processes, two pronounced steps at $e\Phi = 2\bar{\epsilon}_1$ and $e\Phi = 2(\bar{\epsilon}_2 + U_{12})$ that correspond to the onset of resonant transport processes through the first and the second electronic state.

3.3.3 Mode-selective vibrational excitation As our discussion of vibrational rectification effects in Sec. 3.3.2 showed, the effect of cooling by electron-hole pair creation processes can be controlled by the external bias voltage Φ if the molecule is asymmetrically coupled to the leads. Thereby, we focused on the electrical transport properties. In this section, we investigate junctions with multiple vibrational degrees of freedom and describe how the excitation levels of these modes can be selectively controlled exploiting the bias dependence of electron-hole pair creation processes [20, 21]. Such mode-selective vibrational excitation may lead, for example, to applications in mode-selective chemistry [57, 8], where one seeks to break a specific (not necessarily the weakest) chemical bond in a molecule.

To this end, we consider a generic model for a molecular junction with two electronic states and two vibrational modes (model MSVE, see Tab. 2). The two states are located above and below the Fermi level of the junction and may represent, for example, the HOMO and the LUMO level of the molecule. Moreover, the two states are coupled more strongly to the left than to the right lead. Such a coupling scenario is fairly common, in particular if one uses a scanning tunneling microscope to establish the contact to the molecule. The two modes are assumed to couple to one of the two states only, that is $\lambda_{m,\alpha} \sim \delta_{m\alpha}$. This is an idealized situation, which allows to discuss the generic effect. Off-diagonal electronic-vibrational coupling diminishes the effect, which, nevertheless, extends over a wide

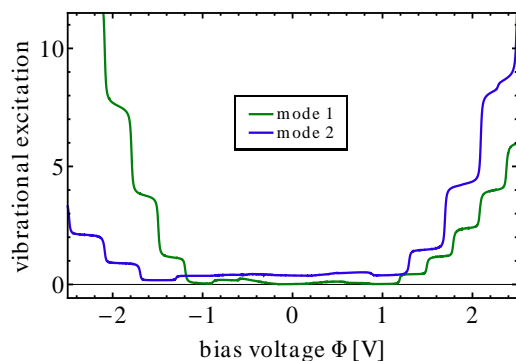


Figure 11 Vibrational excitation characteristics of junction MSVE (cf. Tab. 2).

range of parameters (see Ref. [21] for a more detailed discussion, including the effect of electron-electron interactions).

The vibrational excitation characteristic of the two vibrational modes is depicted in Fig. 11. In particular, mode 1 shows significantly higher levels of excitation than mode 2 for negative and vice versa for positive bias voltages, that is, the excitation levels of the two modes can be selectively controlled by the external bias voltage [20,21]. This can be explained by the same arguments that have been used to analyze the asymmetric excitation levels observed in junction REC (cf. Sec. 3.3.2), because the subsystem consisting of state 1 and mode 1 is effectively decoupled from the subsystem consisting of state 2 and mode 2. Thereby, it should be noted that the frequency of mode 2 is significantly larger than that of mode 1. This means that for positive bias voltages the (current-induced) vibrational energy is distributed in a way that is opposite to what statistical arguments would give in equilibrium systems. In more practical terms, the stronger bond of the molecule, which is associated with mode 2, may eventually break in this junction before the weaker bond. Note that such mode-selective vibrational excitation occurs also for other molecule-lead coupling scenarios [21].

3.3.4 Temperature dependence of the current in the presence of destructive interference effects

Electron-hole pair creation processes play also an important role if electron transport through a single-molecule junction is influenced by quantum interference effects [16, 4, 17]. Quantum interference effects in molecular junctions are of interest not only from a fundamental point of view but also in the context of technological device applications, including transistors [58], thermoelectric devices [59] or spin filters [60]. Interference effects occur in single-molecule junctions, e.g., when electron transport through the junctions is mediated by quasidegenerate electronic states. In this section, we consider an example of such a molecular junction that includes a pair of quaside-

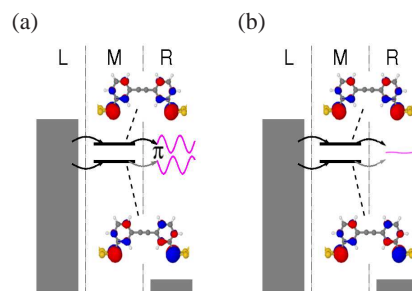


Figure 12 Panel (a) and (b): Graphical representation of a pair of quasidegenerate electronic states. Due to the different $L \leftrightarrow R$ symmetry of the two states, the tunneling amplitudes for (electronic) transport processes through these two states, which are depicted by purple wiggly lines, differ by a phase π . Accordingly, they destructively interfere with each other, resulting in a suppression of the corresponding tunneling amplitude.

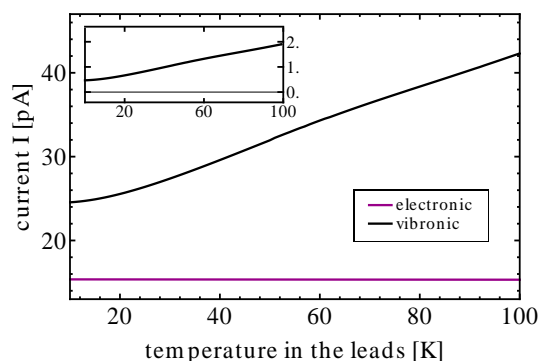


Figure 13 (Color online) Current-temperature characteristics of junction INT (cf. Tab. 2).

generate states: a bonding (symmetric) and an antibonding (antisymmetric) state (model INT, cf. Tab. 2). Note that the symmetry of the two states is reflected in the different sign of the molecule-lead coupling strength $\nu_{R,2}$.

Due to the different symmetry of the two states, the tunneling amplitudes that are associated with electron tunneling through the two states differ by a phase π and, therefore, destructively interfere with each other (see Fig. 12a and 12b). This leads to a strong suppression of the tunnel current in this system [61]. For example, at $e\Phi = 0.2$ eV, the electronic current level of junction INT is given by

$\approx 15 \text{ pA}^2$, while one obtains a current level of $0.4 \mu\text{A}$ if interference effects are discarded in this system.

As we have shown recently, electronic-vibrational coupling can strongly quench such interference effects [16, 17]. Thereby, it is decisive to note that the electronic states of a molecular junction couple differently to the vibrational degrees of freedom, even if they represent just symmetric and antisymmetric combinations of localized molecular orbitals such as, for example, the states depicted in Fig. 12. Thus, due to the interaction with the vibrational degree of freedom, tunneling through one of the states becomes more favorable than through the other and, consequently, interference effects are less pronounced. As a result, the current level of junction INT is significantly larger than without electronic-vibrational coupling. This can be seen in Fig. 13, where the solid black and purple line depict the current-temperature characteristic of junction INT at $e\Phi = 0.2 \text{ eV}$ for the vibronic and electronic transport scenario, respectively.

Thereby, the current level of the electronic scenario shows no temperature dependence because at bias voltages $e\Phi \gg 2\bar{\epsilon}_1$ thermal broadening in the electrodes has no influence on the current level of the junction. In contrast, the vibronic current increases almost linearly with the temperature in the electrodes. This temperature dependence is due to the effect of electron-hole pair creation processes (Fig. 5) [17]. As these processes involve only one of the electrodes, they are not suppressed by destructive interference effects. Therefore, the level of vibrational excitation is determined by electron-hole pair creation processes in this system rather than by inelastic transport processes that are suppressed by destructive interference effects. Similar as for a molecule that is adsorbed on a surface, pair creation processes adapt the vibrational excitation level of the molecule to the temperature in the electrodes, leading to an almost linear increase of vibrational excitation, which is shown in the inset of Fig. 13, as the temperature in the electrodes increases. As a result of the higher excitation levels, inelastic transport processes become more favorable, leading to larger current levels in this system due to an enhanced quenching of destructive interference effects. Thus, electron-hole pair creation processes facilitate a mechanism to control quantum interference effects in this junction by an external parameter, *i.e.* the temperature in the leads. This mechanism has recently been verified in a series of experiments on various single-molecule junctions by S. Ballmann *et al.* [4].

4 Conclusions The theoretical studies [25, 10, 20, 14, 22, 16, 21, 23, 17] of vibrationally coupled electron transport reviewed in this paper show that electron-hole pair

² Note that in this section, Sec. 3.3.4, we refer to the electronic scenario as to the one without electronic-vibrational but including the polaron-shift of the electronic levels. Thus, the level of quasi-degeneracy between the electronic states in the vibronic and the electronic transport scenario is the same.

creation processes play an important role in this nonequilibrium transport problem, although they are not directly contributing to the current that is flowing through the junction. Similar to scenarios where a molecule is adsorbed on a surface, pair creation processes tend to adapt the vibrational excitation levels of the molecular bridge to the temperature in the electrodes. They are directly influencing the vibrational excitation levels of the junction and, thus, also the efficiency of transport processes. Although this represents an indirect influence on the electrical transport properties of a molecular junction it can, nevertheless, lead to a number of interesting transport phenomena such as, for example, negative differential resistance [14] and rectification [14, 21]. In contrast to transport processes, electron-hole pair creation processes involve only one of the electrodes. As a consequence they transfer an asymmetry in the molecule-lead coupling to the corresponding transport characteristics. This is of relevance for spectroscopic applications of single-molecule junctions [23], mode-selective vibrational excitation [20, 21] or in the presence of destructive quantum interference effects [4, 17]. Moreover, it was shown that the suppression of electron-hole pair creation processes leads to higher levels of vibrational excitation in systems with weaker electronic-vibrational coupling [14] and that the absence of electron-hole pair creation processes represents a link between the limit of high bias voltages and weak electronic-vibrational coupling (for $\Phi > 2(\bar{\epsilon}_1 + \Omega_1)$) [22].

Throughout the article, we have focused on resonant processes. It should be noted though, that, similar to resonant and non-resonant transport processes [62, 25], off-resonant electron-hole pair creation processes are also of importance in molecular junctions. Aspects and implications of these processes are discussed, for example, in Ref. [21], where it is shown that they play an important role in the non-resonant transport regime of a molecular junction but also at high bias voltages.

Acknowledgement We thank R. Volkovich, S. Wagner, S. Ballmann, O. Godsi, D. Brisker Klaiman, S. Klaiman, M. Butzin, I. Pshenichnyuk, O. Rubio-Pons, P. B. Coto, B. Kubala, M. Cizek, A. Nitzan and H. B. Weber for many fruitful and inspiring discussions. The generous allocation of computing time by the computing centers in Erlangen (RRZE), Munich (LRZ), and Jülich (JSC) is gratefully acknowledged. This work has been supported by the German-Israeli Foundation for Scientific Development (GIF) and the Deutsche Forschungsgemeinschaft (DFG) through SPP 1243, the Cluster of Excellence 'Engineering of Advanced Materials' and SFB 953. MT gratefully acknowledges the hospitality of the Institute of Advanced Studies at the Hebrew University Jerusalem within the workshop on molecular electronics and the Pitzer Center for Theoretical Chemistry of the University of California at Berkeley. RH is grateful for financial support by

the National Science Foundation (DMR-1006282) and the Alexander von Humboldt Foundation.

References

- [1] J. C. Cuevas and E. Scheer, *Molecular Electronics: An Introduction To Theory And Experiment* (World Scientific, Singapore, 2010).
- [2] E. A. Osorio, K. O'Neill, M. Wegewijs, N. Stuhr-Hansen, J. Paaske, T. Bjørnholm, and H. S. J. van der Zant, *Nano Lett.* **7**, 3336 (2007).
- [3] C. M. Guedon, H. Valkenier, T. Marcussen, K. S. Thygesen, J. C. Hummelen, and S. J. van der Molen, *Nature Nanotechnology* **7**, 305 (2012).
- [4] S. Ballmann, R. Härtle, P. B. Coto, M. Elbing, M. Mayor, M. R. Bryce, M. Thoss, and H. B. Weber, *Phys. Rev. Lett.* **109**, 056801 (2012).
- [5] D. Secker, S. Wagner, S. Ballmann, R. Härtle, M. Thoss, and H. B. Weber, *Phys. Rev. Lett.* **106**, 136807 (2011).
- [6] Y. Kim, H. Song, F. Strigl, H. F. Pernau, T. Lee, and E. Scheer, *Phys. Rev. Lett.* **106**, 196804 (2011).
- [7] M. Galperin, M. A. Ratner, and A. Nitzan, *J. Phys.: Condens. Matter* **19**, 103201 (2007).
- [8] J. I. Pascual, N. Lorente, Z. Song, H. Conrad, and H. P. Rust, *Nature* **423**, 525 (2003).
- [9] G. Schulze, K. J. Franke, A. Gagliardi, G. Romano, C. S. Lin, A. Da Rosa, T. A. Niehaus, T. Frauenheim, A. Di Carlo, A. Pecchia, and J. I. Pascual, *Phys. Rev. Lett.* **100**, 136801 (2008).
- [10] R. Härtle, C. Benesch, and M. Thoss, *Phys. Rev. Lett.* **102**, 146801 (2009).
- [11] M. Galperin, K. Saito, A. V. Balatsky, and A. Nitzan, *Phys. Rev. B* **80**, 115427 (2009).
- [12] A. K. Hüttel, B. Witkamp, M. Leijnse, M. R. Wegewijs, and H. S. J. van der Zant, *Phys. Rev. Lett.* **102**, 225501 (2009).
- [13] G. Romano, A. Gagliardi, A. Pecchia, and A. Di Carlo, *Phys. Rev. B* **81**, 115438 (2010).
- [14] R. Härtle and M. Thoss, *Phys. Rev. B* **83**, 115414 (2011).
- [15] D. R. Ward, D. A. Corley, J. M. Tour, and D. Natelson, *Nature Nanotechnology* **6**, 33 (2011).
- [16] R. Härtle, M. Butzin, O. Rubio-Pons, and M. Thoss, *Phys. Rev. Lett.* **107**, 046802 (2011).
- [17] R. Härtle, M. Butzin, and M. Thoss, *Phys. Rev. B* **87**, 085422 (2013).
- [18] G. Kießlich, E. Schöll, T. Brandes, F. Hohls, and R. J. Haug, *Phys. Rev. Lett.* **99**, 206602 (2007).
- [19] B. N. J. Persson and H. Ueba, *Surface Science* **502-503**, 18–25 (2002).
- [20] R. Härtle, R. Volkovich, M. Thoss, and U. Peskin, *J. Chem. Phys.* **133**, 081102 (2010).
- [21] R. Volkovich, R. Härtle, M. Thoss, and U. Peskin, *Phys. Chem. Chem. Phys.* **13**, 14333 (2011).
- [22] R. Härtle and M. Thoss, *Phys. Rev. B* **83**, 125419 (2011).
- [23] R. Härtle,), *Vibrationally Coupled Electron Transport through Single-Molecule Junctions*, PhD thesis, available online at "<http://www.opus.ub.uni-erlangen.de/opus/volltexte/2012/3316/>", Friedrich-Alexander-Universität Erlangen-Nürnberg, 2012.
- [24] M. Galperin, A. Nitzan, and M. A. Ratner **73**, 045314 (2006).
- [25] R. Härtle, C. Benesch, and M. Thoss, *Phys. Rev. B* **77**, 205314 (2008).
- [26] L. S. Cederbaum and W. Domcke, *J. Chem. Phys.* **60**, 2878 (1974).
- [27] C. Benesch, M. Cizek, M. Thoss, and W. Domcke **430**, 355 (2006).
- [28] E. A. Osorio, M. Ruben, J. S. Seldenthuis, J. M. Lehn, and H. S. J. van der Zant, *Small* **6**, 174 (2010).
- [29] M. Cizek, M. Thoss, and W. Domcke **70**, 125406 (2004).
- [30] A. Mitra, I. Aleiner, and A. J. Millis, *Phys. Rev. B* **69**, 245302 (2004).
- [31] W. Domcke, D. R. Yarkony, and H. Köppel, *Conical Intersections: Electronic Structure, Dynamics and Spectroscopy* (World Scientific, Singapore, 2004).
- [32] A. Groshev, T. Ivanov, and V. Valtchinov, *Phys. Rev. Lett.* **66**, 1082 (1991).
- [33] J. P. Bergfield and C. A. Stafford, *Phys. Rev. B* **79**, 245125 (2009).
- [34] Y. Meir and N. S. Wingreen **68**, 2512 (1992).
- [35] H. Wang, I. Pshenichnyuk, R. Härtle, and M. Thoss, *J. Chem. Phys.* **135**, 244506 (2011).
- [36] T. Böhler, J. Grebing, A. Mayer-Gindner, H. Löhneysen, and E. Scheer, *Nanotechnology* **15**, 465 (2004).
- [37] M. Elbing, R. Ochs, M. Koentopp, M. Fischer, C. von Hänisch, F. Weigend, F. Evers, H. Weber, and M. Mayor **102**, 8815 (2005).
- [38] S. Sapmaz, P. Jarillo-Herrero, Y. M. Blanter, and H. S. J. van der Zant, *New J. Phys.* **7**, 243 (2005).
- [39] N. J. Tao, *Nat. Nano.* **1**, 173 (2006).
- [40] Z. K. Keane, J. W. Ciszek, J. M. Tour, and D. Natelson, *Nano Lett.* **6**, 1518 (2006).
- [41] S. Ballmann, W. Heringer, D. Secker, Q. Zheng, J. A. Gladysz, A. Görling, and H. B. Weber, *ChemPhysChem* **11**, 2256 (2010).
- [42] Y. Xue and M. A. Ratner **68**, 115406 (2001).
- [43] F. Evers, F. Weigend, and M. Koentopp **69**, 235411 (2004).
- [44] C. Benesch, M. Cizek, J. Klimes, M. Thoss, and W. Domcke, *J. Phys. Chem. C* **112**, 9880 (2008).
- [45] C. Benesch, M. F. Rode, M. Cizek, R. Härtle, O. Rubio-Pons, M. Thoss, and A. L. Sobolewski, *J. Phys. Chem. C* **113**, 10315 (2009).
- [46] C. R. Arroyo, T. Frederiksen, G. Rubio-Bollinger, M. Vélez, A. Arnau, D. Sánchez-Portal, and N. Agrait, *Phys. Rev. B* **81**, 075405 (2010).
- [47] J. Koch, M. Semmelhack, F. von Oppen, and A. Nitzan, *Phys. Rev. B* **73**, 155306 (2006).
- [48] R. Avriller, *J. Phys.: Condens. Matter* **23**, 105301 (2011).
- [49] T. P. E. Broekaert, B. Brar, J. P. A. van der Wagt, A. C. Seabaugh, T. S. Moise, F. J. Morris, E. A. Beam, and G. A. Frazier, *IEEE J. Solid State Circ.* **33**, 1342 (1998).
- [50] P. Mazumder, S. Kulkarni, M. Bhattacharya, J. P. Sun, and G. I. Haddad, *Proc. IEEE* **33**, 596 (1998).
- [51] R. H. Mathews, J. P. Sage, T. C. L. Gerhard Sollner, S. D. Calawa, C. L. Chen, L. J. Mahoney, P. A. Maki, and K. M. Molvar, *Proc. IEEE* **87**, 596 (1999).
- [52] J. H. Davies, S. Hershfield, P. Hyldgaard, and J. W. Wilkins, *Phys. Rev. B* **47**, 4603 (1993).
- [53] J. H. Davies, S. Hershfield, P. Hyldgaard, and J. W. Wilkins, *Ann. Phys. (NY)* **236**, 1 (1994).
- [54] D. Boese and H. Schoeller **54**, 668 (2001).

- [55] A. Zazunov, D. Feinberg, and T. Martin, *Phys. Rev. B* **73**, 115405 (2006).
- [56] V. Mujica, M. A. Ratner, and A. Nitzan, *Chem. Phys.* **281**, 147 (2002).
- [57] J. Jortner, R. D. Levine, and B. Pullman, *Mode-selective chemistry* (Kluwer, Amsterdam, 1991).
- [58] C. A. Stafford, D. M. Cardamone, and S. Mazumdar, *Nanotechnology* **18**, 424014 (2007).
- [59] J. P. Bergfield, M. A. Solis, and C. A. Stafford, *ACS Nano* **4**, 5314 (2010).
- [60] C. Herrmann, G. C. Solomon, and M. A. Ratner, *J. Chem. Phys.* **134**, 224306 (2011).
- [61] G. C. Solomon, D. Q. Andrews, T. Hansen, R. H. Goldsmith, M. R. Wasielewski, R. P. Van Duyne, and M. A. Ratner, *J. Chem. Phys.* **129**, 054701 (2008).
- [62] M. C. Lüffe, J. Koch, and F. von Oppen, *Phys. Rev. B* **77**, 125306 (2008).